Chapter 10

Microstructure Engineering of Metal-Halide Perovskite Films for Efficient Solar Cells

Weidong Zhu, Jingjing Chang, Chunfu Zhang, Jincheng Zhang and Yue Hao

Additional information is available at the end of the chapter

http://dx.doi.org/10.5772/intechopen.74225

Abstract

Photovoltaic (PV) devices with metal-halide perovskite films, namely perovskite solar cells, have become a rapidly rising star due to low cost of raw materials, simple solution processability, and swiftly increased power conversion efficiency (PCE). The PCEs so far certified have gone beyond 22% for perovskite solar cells and 23.6% for tandem devices with single crystalline silicon solar cells, which offer a promising PV technology for practical applications. In principle, performance of perovskite solar cells are largely dominated by the optoelectronic properties and stability of metal-halide perovskite films, which are determined by the microstructure features of the films in turns. In this chapter, we will describe the recently developed strategies on microstructure engineering of metal-halide perovskite films for efficient perovskite solar cells.

Keywords: metal-halide perovskites, polycrystalline film, microstructure engineering, power conversion efficiency, solar cells

1. Introduction

Photovoltaic (PV) devices with metal-halide perovskites that follow the formula of ABX_3 [$A = H_3NH_3$ (MA), $NH = CHNH_3$ (FA), or Cs; B = Pb, Sn; X = I, Br, and Cl] or their alloyed counterparts [1, 2], namely perovskite solar cells, have swiftly emerged as a focal point of PV community owing to their low-cost, easy and large-scale fabrication, swiftly improved power conversion efficiency (PCE) to over 22% from 3.8% in just few years [3], and feasibility of tandem with well-developed PV technologies [4]. Those combined merits basically come from exceptional optoelectronic features of metal-halide perovskite films such as high absorption

coefficient, tunable bandgap, long and balanced carrier diffusions, ambipolar transport of charge carriers, tolerance of defects [5, 6], along with widely available raw materials and feasibility of film deposition via solution routes.

Critical to fabrication of efficient perovskite solar cells is deposition of high-quality metal-halide perovskite films with tailored microstructural features that mainly refer to surface coverage, grain size, texture, surface roughness, and so on [7, 8]. All of them are previously revealed to play extremely important roles for ultima device performance and even stability. For example, as for surface coverage of metal-halide perovskite films, Snaith et al. [9] revealed that the lowest average efficiency is observed for the lowest coverage of $MAPbI_{3-x}Cl_x$ film, and vice versa. In terms of grain size of metal-halide perovskite films, Huang et al. [10] demonstrated that solvent annealing route can effectively increase the grain size and crystallinity of $MAPbI_3$ films, which resulted in much improved material electronic property and device performance. Similarly, Ohkita et al. [11] showed that the cells exhibited improved PV parameters with increase of grain size of $MAPbI_3$ films. In particular, reduced trap-assisted recombination resulted from large-sized grains gave rise to high open-circuit voltage (V_{oc}) for the cells. In addition, Park et al. [12] declared that as $MAPbI_3$ grain size decreases, the photocurrent density-voltage (J-V) hysteresis of perovskite solar cells tended to be more obvious. On the part of texture of metal-halide perovskite films, Jo et al. [13] successfully fabricated $MAPbI_3$ films with two different crystal orientations with respect to the substrate by using two different organic precursors (MAI and MACl). They found that the PV performance is directly related to crystal orientation of $MAPbI_3$ due to anisotropy of charge transfer in the crystal, suggesting that control of crystal orientation of metal-halide perovskites is important to realize high-performance cells. With regard to surface roughness, Kwok et al. [14] prepared a bilayer-structured $MAPbI_3$ film, which is compose of a mesostructured underlayer and a dense upper layer. They revealed that higher V_{oc} of cell is directly related to smaller root mean squares (RMS) of $MAPbI_3$ upper layer. Overall, a metal-halide perovskite film with the desired microstructures of full surface coverage, large grain size, textured feature, and smooth surface, is highly desirable for efficient perovskite solar cells.

At this point, much research attention has been focused on microstructure engineering of metal-halide perovskite films. In the past year, there have been rapid progresses in this research field. Therefore, in this chapter we will focus our attention on the review of recently developed strategies on microstructure engineering of metal-halide perovskite films aiming to realize high-performance and stable perovskite solar cells. In particular, in the first section we begin with a general introduction to basic fundamentals of metal-halide perovskite materials that used as the absorbers for solar cells. In the second section, we come to the discussion of deposition technologies of metal halide perovskite films. And in the third section, we will discussion the recently developed strategies toward the microstructure engineering of metal-halide perovskite films by modifying the deposition technologies of metal halide perovskite films.

2. Basic fundamentals of metal-halide perovskites for solar cells

2.1. Crystal structures

The mineral perovskite named for Russian mineralogist Lev Perovski, possesses the chemical formula of $CaTiO_3$. Compounds with the same crystal structure, i.e., ABX_3 are called

http://dx.doi.org/10.5772/intechopen.74225

perovskites. For a cubic unit cell, eight corners of the cube are occupied by A-cations and a B-cation is resided in its body center. The B-cation is encircled by six X-anions that located at the face centers of the cube unit cell. The six X-anions and one B cation form an octahedral $[MX_6]^{4-}$ cluster. By changing the element types at A and/or B sites, we can obtain the perovskite variants with a variety of physical properties, such as semiconductive, superconductive, ferroelectric, antiferroelectric, etc. [16]. For the ones used for solar cells, the large cation at A site is commonly chosen to be organic cations such as methylammonium (MA, $CH_3NH_3^+$), formamidinium (FA, $HC(NH_2)_2^+$), phenylammonium (PhA, $C_2H_5NH_3^+$), or inorganic Cs^+ cation [17, 18], as shown in **Figure 1(a)**. A polar organic cation can yield a larger dielectric constant than an all inorganic system. However, organic cations are companied by poor stability of the compounds [19]. A large atom of Pb or Sn is generally settled down at B site, which then couples with halide X anions including Cl^-, Br^-, and I^- to form metal-halide perovskite. By designing the component ratios, a series of metal-halide perovskite variants can be realized, which thus suggests an interesting and effective way to develop new materials [20]. In addition, replacing the halide at X sites with BF^{4-}, PF^{6-}, or SCN^- can also engineer the materials' properties; especially in boosting their stability [17].

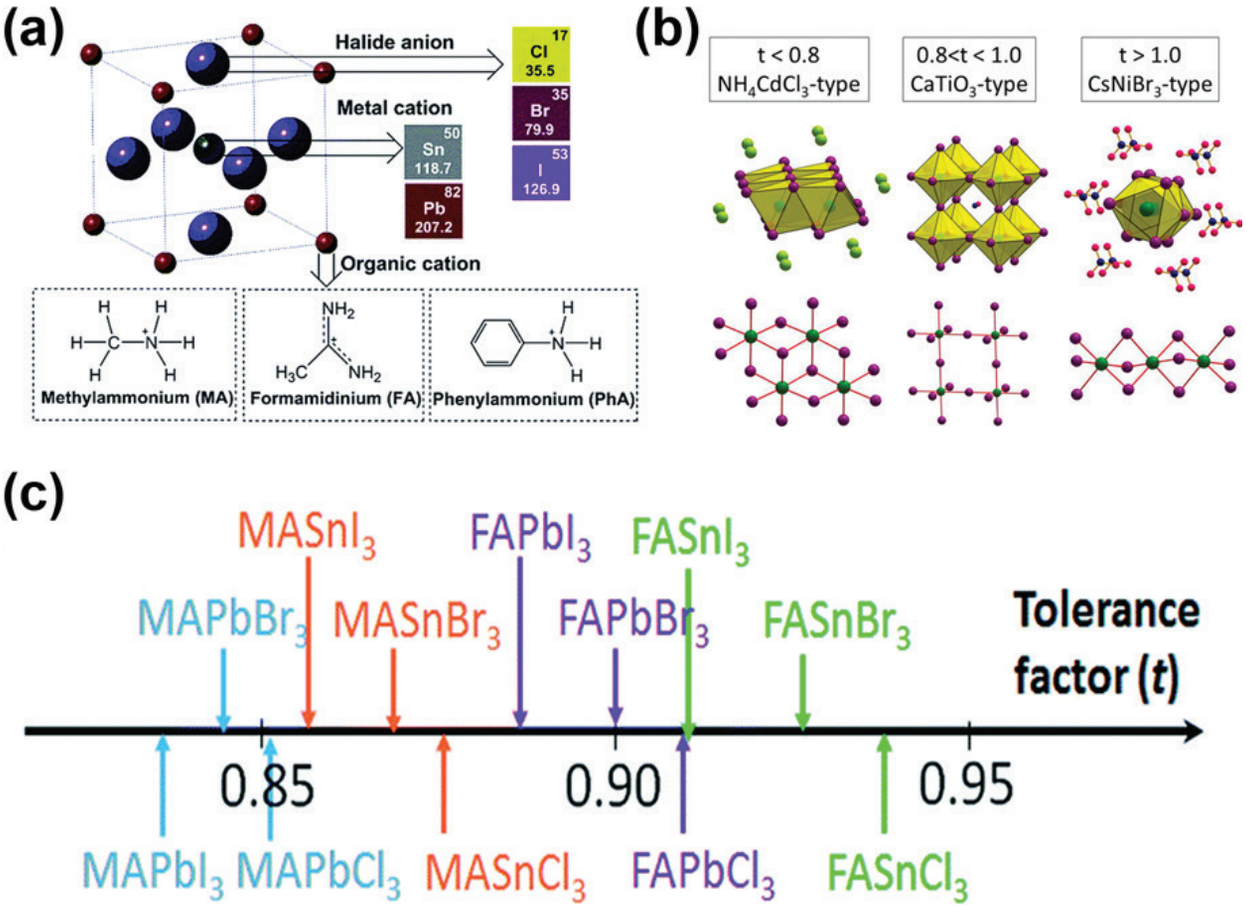

Figure 1. (a) Schematic crystal structure of metal-halide perovskites. Reproduced with permission from Ref. [17]. Copyright 2015, Royal Society of Chemistry. (b) Structural motifs for ABX_3 metal-halide perovskites as a function of the ionic radii of A^+, B^{2+}, and X^- ions expressed with a tentative tolerance factor value. Reproduced with permission from ref. [22]. Copyright 2015, American Chemical Society. (c) Tolerance factors (t) of a series of metal-halide perovskites. Reproduced with permission from Ref. [15]. Copyright 2015, Royal Society of Chemistry.

The structural formability and stability of metal-halide perovskites is guided by its geometric tolerance factor (t), $t = (r_A + r_X)/[\sqrt{2}(r_B + r_X)]$, where r_A, $r_{B,}$ and r_X are the effective ionic radii of A, B, and X, respectively [21]. As indicated in **Figure 1(b)**, for the ones with t close to 1, they prefers an ideal cubic structure, while they distorts into a low-symmetry structure, when t is smaller than 1. And, the ones with t value between 0.8 and 1.0 tend to adopt a cubic structure, and photo-inactive non-perovskite structures are formed when the value of t is larger (>1) or smaller (<0.8) [22]. **Figure 1(c)** gives the estimated t of a series of metal-halide perovskites [23]. We can see that all the values are in the range of 0.8–1, which is a universal feature of perovskite structure. Replacing Pb with Sn appears to be beneficial to increase t; yet it induces the serious decrease of the compound stability. This mainly comes from the fact that t is not the only determinant factor, and Pb is inerter to oxidization than Sn [6]. In addition, as for organic cation, it seems that both charge distribution and size dominant the crystal structure. Previous works revealed that MA and FA benefit to stabilized perovskite structure, while the others with similar size, such as $CH_3CH_2NH_3^+$, $(CH_3)_2NH_2^+$ are easily induce the formation of a non-perovskite structure [22].

At different temperatures, a metal-halide perovskite crystal usually exhibits α, β and γ phases, as schematized in **Figure 2** [24]. For example, the α to β phase transition for $MAPbI_3$ happens at 330 K, while the β to γ phase transition appears at 160 K. Noting that a non-perovskite δ phase was also found in some metal-halide perovskite variants such as $HC(NH_2)_2PbI_3$, $FAPbI_3$, $CsPbI_3$, and $CsSnI_3$. The B–X bond of δ phase is broken. So it cannot be derived from the α phase by B–X–B bond angle distortion [25].

2.2. Electronic structures

Electronic band structures of metal-halide perovskites were initially investigated by Koutselas et al. [26] using band structure calculations. Then, Umebayashi et al. [27] studied the electronic band structures of cubic phase metal-halide perovskites based on ultraviolet photoelectron spectroscopy and first principles density functional theory (DFT) band calculation. It has been revealed that valence band maximum (VBM) states of $MAPbX_3$ and $CsPbX_3$ (X = Cl, Br, I) crystals contain Pb 6p-I 5p σ-antibonding orbital, while conduction band minimum (CBM) states compose of Pb 6p-I 5 s σ anti-bonding and Pb 6p-I 5p π antibonding orbitals [27]. Yan et al. [28] conducted the calculations of band structure, partial charge density of VBM and CBM states and (partial) density of states (DOS) of α phase $MAPbI_3$. The results revealed that the direct band-gap locates at the R point. And, Pb has an occupied 6 s orbital below the top of valence bands. This lone pair of s electrons in $MAPbI_3$ maybe accounts for its unique optoelectronic properties. Further, partial charge density and DOS plots indicate that CBM largely compose of Pb p state, while VBM exhibits obvious Pb s and I p antibonding feature. This means that electronic structure of $MAPbI_3$ uniquely has the dual nature of ionic and covalent properties. In addition, the electronic states resulted from the organic cations are away from band edge. It means that organic cations have a negligible impact on basic electronic structures of $MAPbI_3$ [25].

2.3. Optoelectronic properties

2.3.1. Light absorption and bandgap

The feature of strong absorption over a wide range of spectrum is highly desired for absorber material of PV device, which is conductive to enlarge photocurrent, diminish the usage

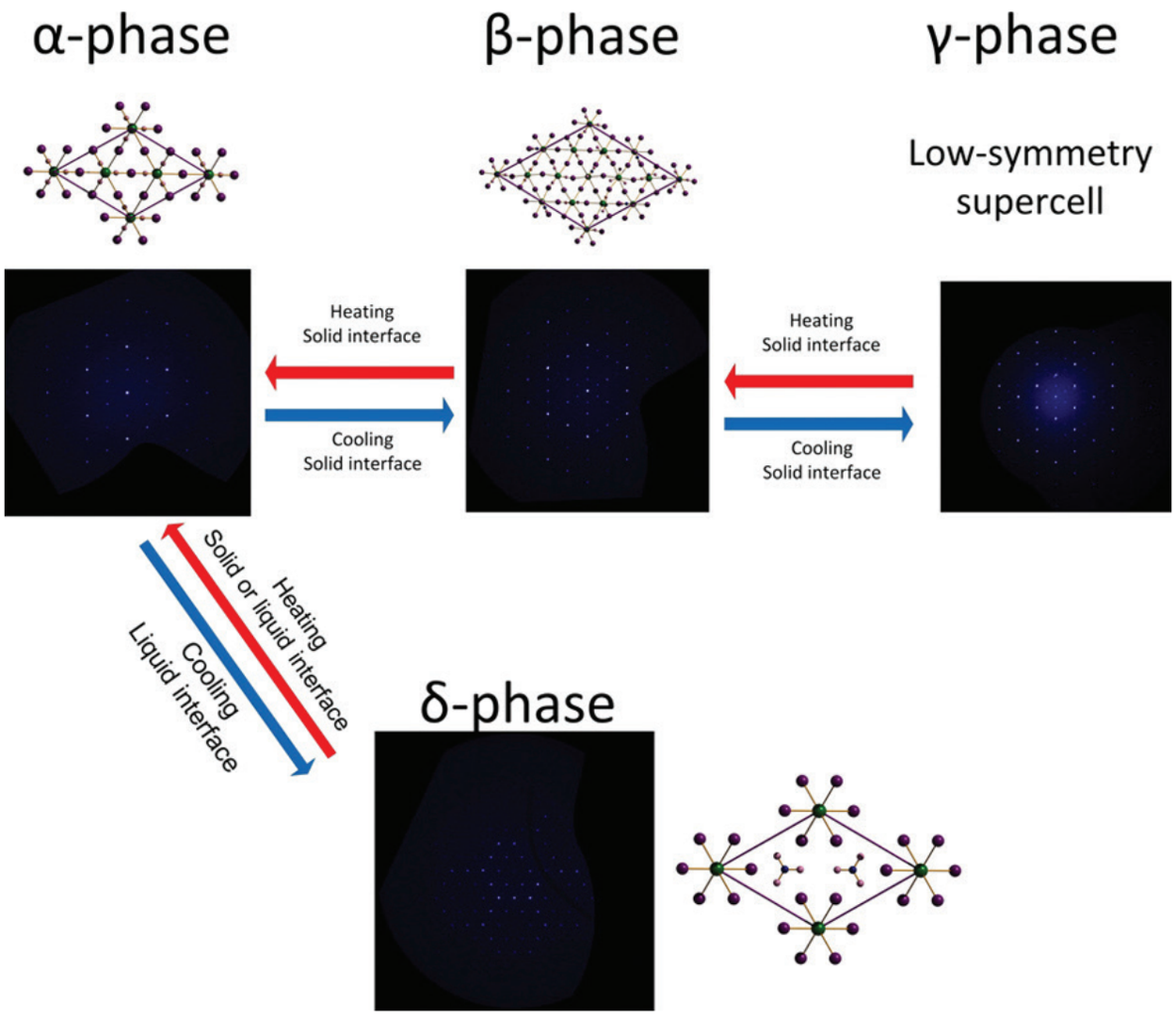

Figure 2. Graphical scheme of phase transitions of $MA(Pb,Sn)X_3$ materials. Precession images are drawn at [006] view. Reproduced with permission from Ref. [24]. Copyright 2013, American Chemical Society.

amount of raw material, and minimize the charge and energy loss during extraction to electrodes [6]. One highlighted property of metal-halide perovskite materials is their very high absorption coefficient along with sharp onset of absorption edge [2]. Moreover, most of metal-halide perovskite materials are direct bandgap semiconductors [28]. In terms of the most typical $MAPbI_3$, its absorption coefficient exceeds 3.0×10^4 cm^{-1} in the visible range, which means that it only needs 380 nm thin film to absorb 90% of the visible light [2]. In fact, the thickness of light absorption layer for most of perovskite solar cells is around 300–600 nm. In addition, $MAPbI_3$ film shows a very sharp absorption onset, which means the low density of deep states of it. The Urbach energy of $MAPbI_3$ film was estimated to as low as 15 meV, which is comparable to monocrystalline GaAs [29]. The sharp absorption onset of $MAPbI_3$ maybe contribute to the small offset between its optical bandgap (~1.55 eV) and V_{oc} of ultimate devices (~1.10 V) [6].

Another unique property of metal-halide perovskites is their bandgap tunability, which can be realized by substituting the atoms at A, B, or X sites. When MA was replaced with a slightly larger FA, the reduced bandgap from 1.55 to 1.48 eV was observed, corresponding to

an absorption edge extended from 800 to 840 nm, as firstly reported by Eperon et al. [30]. And, the photocurrent of the cell with $FAPbI_3$ film can reach up to 23 mA cm^{-2}, because of extended light absorption range. While a smaller Cs^+ at A site gives rise to an increased bandgap of 1.73 eV [31]. For X site, after replacing I^- with Br^- or Cl^-, the bandgap increases to 2.30 eV for $MAPbBr_3$ or 3.12 eV for $MAPbCl_3$, respectively. **Figure 3(a–c)** shows the continuous bandgap variation of $FAPbI_yBr_{3-y}$ ($0 < y < 1$) films. Its absorption onset changes from 840 nm for $FAPbI_3$ to 550 nm for $FAPbBr_3$, corresponding the bandgap increases from 1.48 to 2.13 eV. For B site, a smaller cation size usually results in less bandgap. For example, the bandgap of $MAPbI_3$ decreases to 1.2 eV by replacing the Pb^+ with Sn^+ [24]. Similarly, the bandgap decreases from 1.67 eV for $CsPbI_3$ to 1.30 eV for $CsSnI_3$ and 1.08 eV for $CsGeI_3$ [24].

2.3.2. Long-range ambipolar charge transport

For most of semiconductors, the transport of electrons and holes is unbalanced, due to different effective masses (m_e^* and m_h^*). Surprisingly, numerous independent experimental studies have revealed that well-balanced electron and hole transport is established in metal-halide perovskites, namely ambipolar transport property. First principle calculation also indicates that this fact that electron effective mass ($m_e^* = 0.23\ m_0$) of this type materials is extremely similar to hole effective mass ($m_h^* = 0.29\ m_0$) [32]. Balanced ambipolar transport has an effect on bulk polarization during charge transport and collection; in turns affects PV parameters of perovskite solar cells. Moreover, metal-halide perovskites can convey both n-type and p-type properties when they are used in thin-film devices with different interfacial layers [22]. In addition, long carrier diffusion length of ~100 nm and ~1 μm were revealed

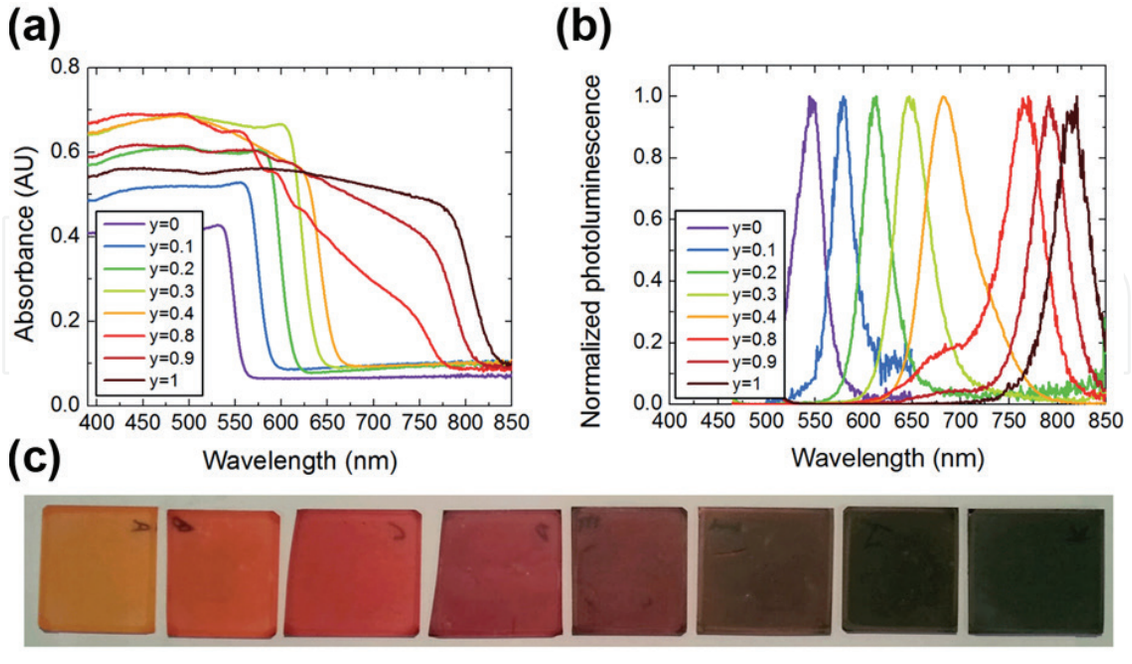

Figure 3. (a) UV-Vis absorbance spectra of $FAPbI_yBr_{3-y}$ metal-halide perovskite films with different y values. (b) Steady-state photoluminescence spectra for the corresponding films. (c) Photographs of the films with y increasing from 0 to 1 (left to right). Reproduced with permission from Ref. [30]. Copyright 2014, Royal Society of Chemistry.

for solution-processed $MAPbI_3$ and $MAPbI_{3-x}Cl_x$ films, which are much larger than that of organic semiconductors. Almost certainly, long diffusion length can bring reduced charge recombination and improved charge collection, thus excellent cell performance [18].

2.3.3. Exciton binding energy

The hybrid nature of metal-halide perovskite materials arise wonders whether incident photons generate free charges or bound excitons. So, the exciton binding energy of metal-halide perovskite materials has been intensively concerned [18]. In the 1990s, theoretical studies have revealed the exciton binding energy to be around 37 meV for $MAPbI_3$ [33]. This value is much lower than that of organic materials with the values ranged from 0.2 to 1 eV. The low binding energy together with long diffusion length maybe account for the high PECs of perovskite solar cells. The low binding energy of metal-halide perovskites is mainly related to their large dielectric constants, which give rise to strong dielectric screening effect [18]. Recently, Hu et al. [34] found that the dielectric constant $MAPbI_3$ is as high as ~32 under dark condition. And, the value can be greatly enhanced (~1000) under photoexcitation as investigated by Juarez-Perez et al. [35]. The high dielectric constant gives rise to strong dielectric screening effect, thus low exciton binding energy.

3. Film formation technologies

Up to now, various processing techniques have been developed to prepare metal-halide perovskite films, as summarized in **Figure 4**. They mainly include one-step spin-coating method, sequential solution deposition method, two-step spin-coating method, vacuum co-evaporation deposition method, sequential vacuum deposition method, and vapor-assisted solution deposition method [36].

The one-step spin-coating method involves spin-coating of a precursor solution containing PbX_2 with a certain amount of MAX firstly (X = I, Br, and Cl). Then, the metal-halide perovskites formed and grew during solvent evaporation. A post-annealing recipe with a temperature of ~100°C was usually required to remove residual solvents and complete crystallization. For this method, the film morphology and quality strongly depend on the processing conditions such as annealing temperature, solution concentration, precursor composition, solvent choice, etc. [36]. Although it is extremely simple, the one-step spin-coating method faces the difficulty to the deposition of pinhole-free metal-halide perovskite films. Solvent engineering is proved to be one of effective routes to overcome this obstacle. Spiccia et al. [37] proposed a fast deposition crystallization method to induce the crystallization of $MAPbI_3$ during spin-coating process. This method includes the spin-coating of $MAPbI_3$ precursor with N,N-dimethylformamide (DMF) as the solvent, followed by dropping anti-solvent such as toluene and chlorobenzene to complete the crystallization of $MAPbI_3$. The anti-solvent decreased the $MAPbI_3$ solubility in DMF solvent, and thereby promoting fast nucleation and crystallization [6]. Later, Jeon et al. [38] designed a mixed γ-butyrolactone and dimethyl sulfoxide (DMSO) as the processing solvent followed by toluene drop-casting. The difference is

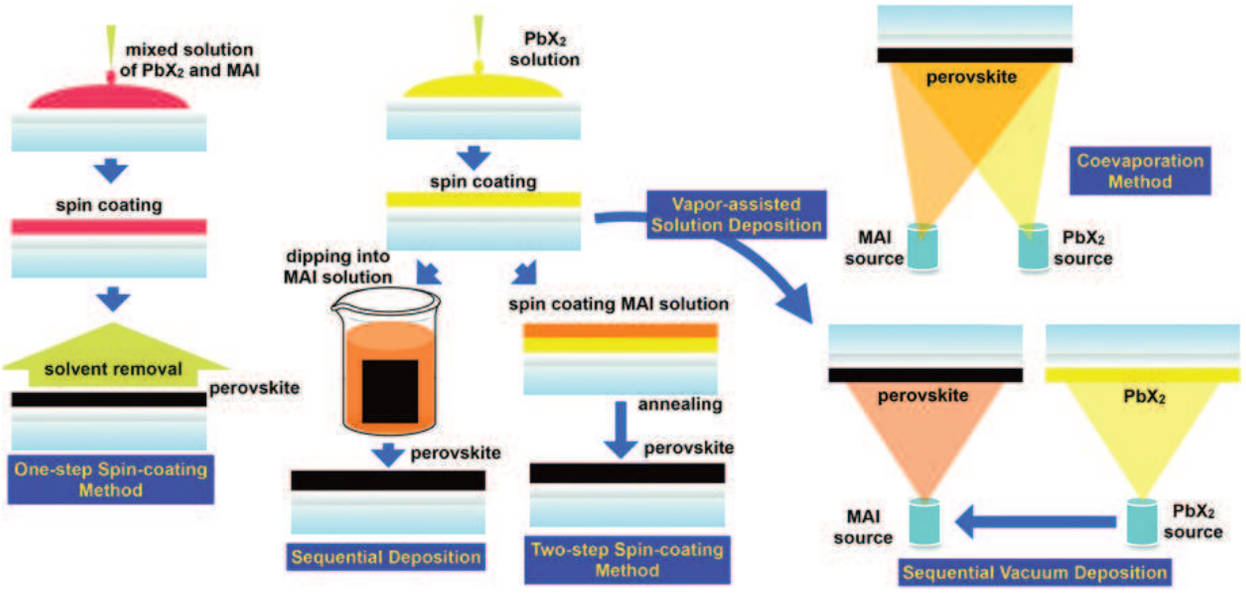

Figure 4. Illustrations of developed processing techniques for deposition of metal-halide perovskite films. Reproduced with permission from Ref. [36]. Copyright 2015, Royal Society of Chemistry.

that a dark brown $MAPbI_3$ film formed immediately after dropping of toluene solvent, while a transparent MAI-PbI_2-DMSO intermediate phase formed firstly after dropping of toluene using the mixed solvent. Both X-ray diffraction (XRD) and Fourier-transform infrared spectroscopy (FTIR) measurements verified the formation of intermediate phase. After being thermal annealed at 100°C for 10 min, intermediate phase film can transform to an extremely uniform and compact $MAPbI_3$ layer [6]. Similarly, Park et al. [39] further developed the intermediate phase route based on Lewis acid adduct of PbI_2, as shown in **Figure 5**. This method eventually resulted in an average PCE of 18.3% from 41 cells and the best value of 19.7%.

The sequential deposition procedure was firstly introduced by Grätzel et al. [40]. And in surprise, it yielded a high PCE of 15%. This method includes the spin-coating of a PbX_2 solution on substrate, followed by drying, and then dipping the substrate into an isopropanol (IPA) solution of MAX to accomplish the reaction in few minutes. Typically, the solutions are 1 M PbI_2 in DMF and MAI in IPA with relative low concentration from 0.004 to 0.006 M. After the dipping step, the residual MAI was rinsed out by IPA. With this method, the films' homogeneity can be dramatically improved and their morphology becomes more controllable than the one-step spin-coating method.

The two-step spin-coating method that is also known as interdiffusion method was proposed by Huang et al. [41]. It can be seen as the one derived from sequential deposition procedure. But, the difference is that metal-halide perovskite is formed by spin-coating an MAI layer on PbX_2 precursor film followed by thermal annealing at 100°C for a relative long time up to 2 h. This method is materials saving, and can synthesize more uniform films than sequential deposition.

Snaith et al. [42] firstly reported the vacuum co-evaporation deposited planar $MAPbI_{3-x}Cl_x$ perovskite solar cells by co-evaporating $PbCl_2$ and MAI in a vacuum thermal evaporation system. The PCEs with a narrow distribution and optimal one of 15.4% were observed in

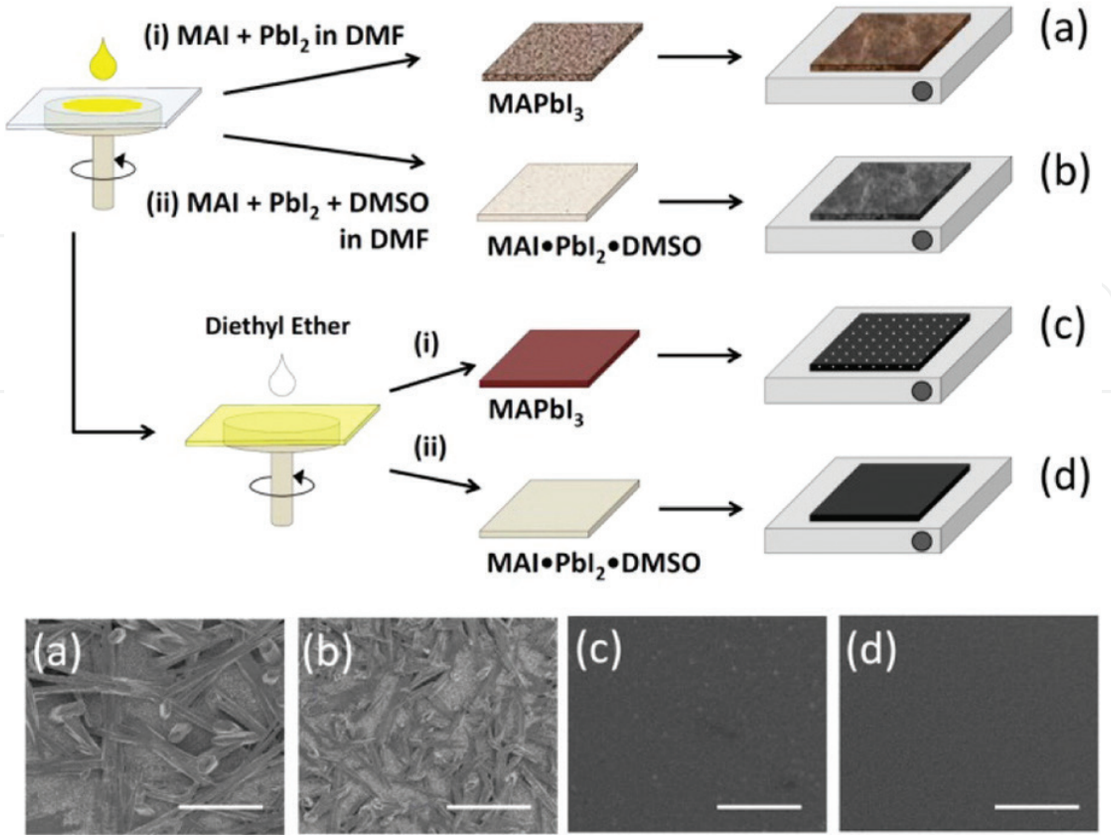

Figure 5. Schematic illustration of processing procedures for $MAPbI_3$ films deposition as well as the corresponding scanning electron microscopy (SEM) images. The $MAPbI_3$ films were deposited by one-step spin-coating of the DMF solution containing (a) MAI and PbI_2 or (b) MAI, PbI_2, and DMSO. Panels (c) and (d) were prepared by same solution as that in panels (a) and (b), but diethyl ether was dripped during the spinning process. Reproduced with permission from Ref. [39] . Copyright 2015, American Chemical Society.

contrast with that of one-step solution process. Due to its low control accuracy in precursor ratio, the sequential vacuum evaporation technology was further developed via depositing $PbCl_2$ and MAI layer by layer [43]. By heating the substrate during precursor evaporation, a pure-phase, homogeneous, and pinhole-free $CH_3NH_3PbI_{3-x}Cl_x$ film can be synthesized. However, the requirement of high vacuum degree of them inevitably increases the device cost, and thus partially restricts their practical applications.

Vapor-assisted solution deposition is firstly used by Yang et al. [44]. For it, PbI_2 film that was pre-deposited via spin-coating route reacted with MAI vapor under atmospheric pressure. The resultant $MAPbI_3$ film was revealed to be extremely smooth, and composed of microscale polycrystallites, delivering to a PCE of 12%.

4. Microstructure engineering of metal-halide perovskite films

The microstructural features of metal-halide perovskite films such as surface coverage, grain size, texture, surface roughness, and so on are previously revealed to play extremely vital

roles for determining ultima device performances and even stability. In the past year, there have been rapid progresses in the research field of microstructure engineering of metal-halide perovskite films. In this section, we will focus our attention on the recently developed strategies on microstructure engineering of metal-halide perovskite films aiming to realize high-performance and stable perovskite solar cells.

4.1. Surface coverage engineering of metal-halide perovskite films

The reasons for ensuring surface coverage of metal-halide perovskite film in perovskite solar cells come from the following two reasons. On the one hand, if there are some regions without metal-halide perovskites padding, light will travel directly without absorption, which leads to decreased photocurrent in turns. On the other hand, any existed pinholes inevitably result in direct contact of electron transport layer with hole transport layer, thus resulting in the formation of shutting paths. They will form additional parallel resistors, causing declines in performance parameters of the cell.

The traditional one-step spin-coating method faces the difficulty to yield a uniform and full-coverage metal-halide perovskite film in large areas. Aiming to overcome this issue, some effective modifications have been reported. For example, as given in **Figure 6(a)**, Yu et al. [45] introduced a recrystallization process via DMF vapor fumigation to induce the self-repair of one-step deposited $MAPbI_3$ films with poor coverage and low crystallinity. By adjusting the cycle of recrystallization process, they found that $MAPbI_3$ films with dendritic structures spontaneously transformed to the uniform ones with full coverage and high crystallinity (**Figure 6(b–e)**). Solar cells with these modified $MAPbI_3$ films yielded reproducible average PCE of 10.25 ± 0.90% and the optimal one of 11.15%, which is both much higher than that of non-modified $MAPbI_3$ films (**Figure 6(f–d)**). In addition, the J-V hysteresis in the measurement of cell performance can also be effectively alleviated. The authors attributed this desired feature to improve the quality of $MAPbI_3$ films in the optimized devices.

Cui et al. [46] discovered that methylamine (CH_3NH_2) gas can trigger defect-healing of $MAPbI_3$ films via room-temperature ultrafast, reversible chemical reaction of $MAPbI_3$ with CH_3NH_2 gas. They revealed that healing of $MAPbI_3$ films can be ascribed to the formation and reconstruction of an intermediate $MAPbI_3{\cdot}xCH_3NH_2$ liquid phase during perovskite-gas interaction. $MAPbI_3$ film processed by one-step spin-coating method using DMF as solvent is composed of dendrite-like $MAPbI_3$ crystals. And voids with size up to several micrometers between them can be clearly found. After CH_3NH_2 induced defect-healing treatment, dendrite-like crystals and voids almost disappeared and a dense, smooth $MAPbI_3$ film has formed. And, AFM measurement further revealed that the healed film has a very dense and smooth surface, with a RMS roughness of ~6 nm. Benefiting from improved surface coverage of $MAPbI_3$ films by methylamine-induced defect-healing, obvious increase of PCE from 5.7 to 15.1% were realized for the cells. Afterwards, this interesting chemical reaction of CH_3NH_2 gas with metal-halide perovskite was investigated in detailed and extended for further uses such as reduction of intrinsic defect concentration of $MAPbI_3$ films [47], realization of solvent- and vacuum-free deposition of $MAPbI_3$ films [48], and so on.

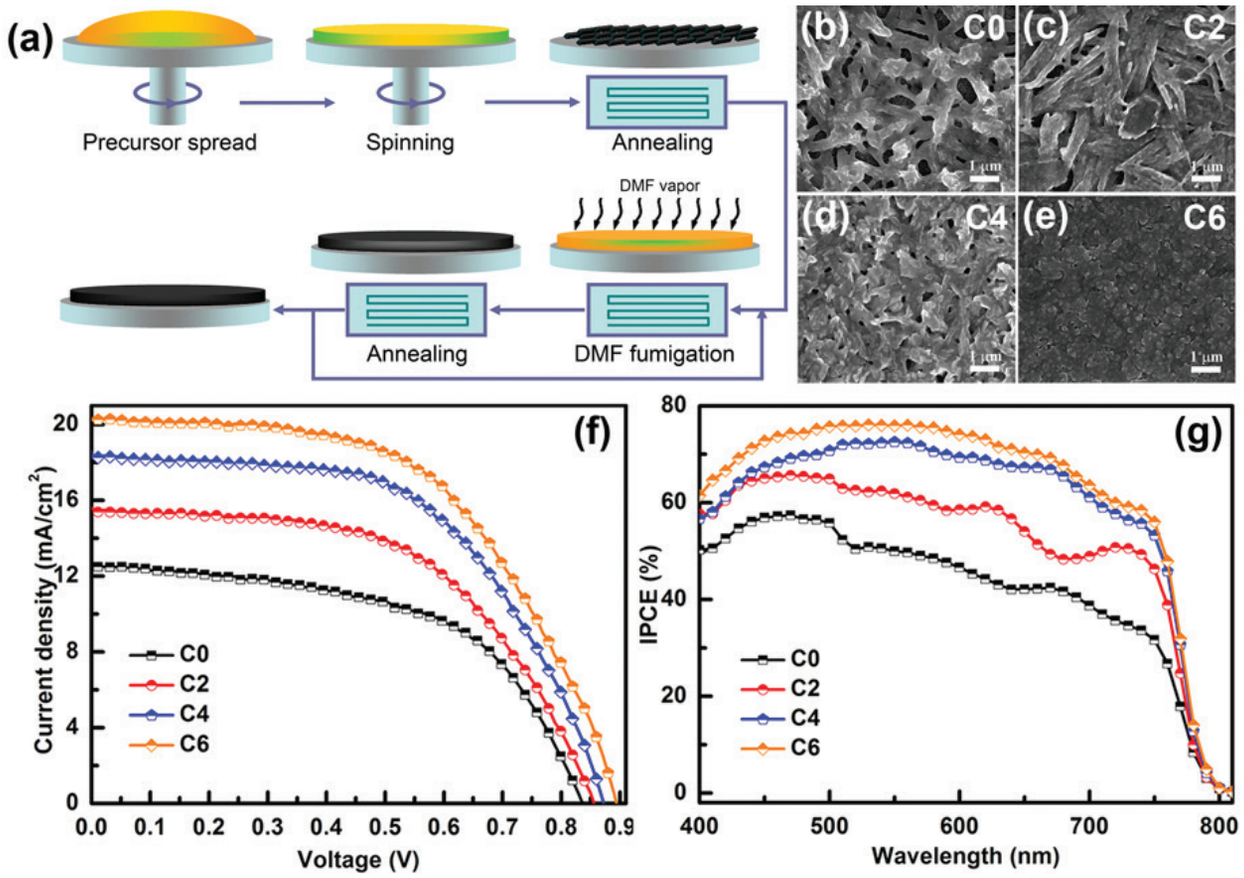

Figure 6. (a) Schematic processing procedure for $MAPbI_3$ film deposition (C0) and recrystallization *via* DMF vapor fumigation for 2 (C2), 4 (C4), and 6 (C6) cycles. (b–e) Surficial SEM images of samples C0, C2, C4, and C6. (f) J-V curves and (g) IPCE spectra of the devices based on samples of C0, C2, C4, and C6, respectively. Reproduced with permission from Ref. [45]. Copyright 2015, Royal Society of Chemistry.

4.2. Grain size engineering of metal-halide perovskite films

Increasing theoretical and experimental evidences indicate that, similar to well-developed thin-film PV devices such as CdTe and $Cu(InGa)Se_2$, primary energy loss in perovskite solar cells is also ascribed to non-radiative recombination of carriers at undesirable trap states. In general, for polycrystalline perovskite films trap states mainly come from crystal imperfections especially such as grain boundaries and intragranular defects [49, 50]. While number of grain boundaries is inversely proportional to average grain size for polycrystalline film, so numerous works have been focused on increasing grain size of metal-halide perovskite films by modifying deposition technologies of metal halide perovskite films.

For example, as shown in **Figure 7**, Yu et al. [49] demonstrated that a homogeneous cap-mediated crystallization with face-to-face configuration can control the crystallization kinetics of $MAPbI_3$ films in one-step spin-coating method. They found that homogeneous caps, especially the ones with low surface roughness, can effectively retard the nucleation rate, promote growth, and prevent composition loss of $MAPbI_3$ grains. Thus, pinhole-free $MAPbI_3$ films can be formed, which have many desirable features, such as greatly enlarged grains, significantly

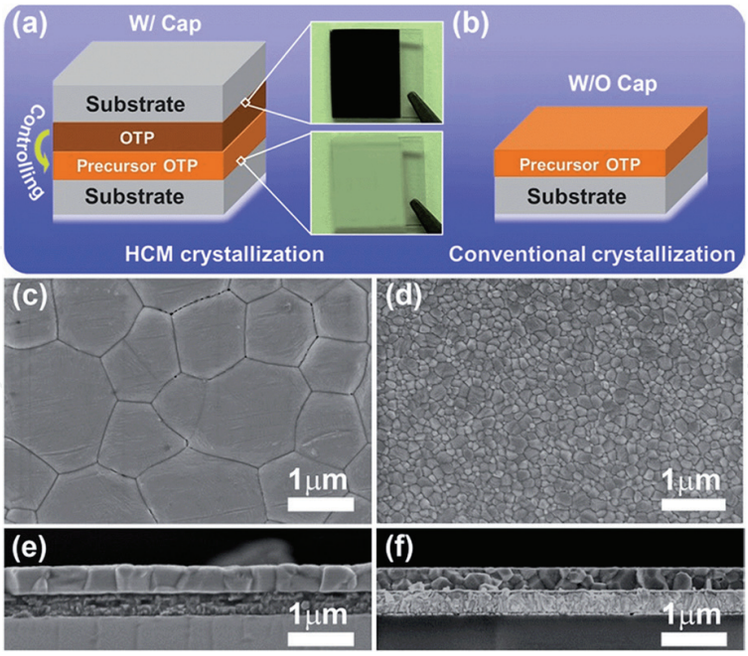

Figure 7. (a) Illustration of homogeneous cap-mediated crystallization configuration, where a crystallized $MAPbI_3$ on TiO_2/FTO substrate is placed face to face on precursor $MAPbI_3$ film. (b) Illustration of conventional crystallization configuration. Top-view and cross-sectional SEM images of $MAPbI_3$ films prepared by (c, e) homogeneous cap-mediated crystallization and (d, f) conventional crystallization, respectively. Reproduced with permission from Ref. [49]. Copyright 2016, Royal Society of Chemistry.

improved crystallinity, preferred (110) orientation, vertically aligned grain boundaries, and proper stoichiometry. As a result, planar-resultant heterojunction solar cells yielded a much enhanced average PCE of 17.87%. It should be noted that large fill factors (FFs) were observed in these efficient cells. In subsequent work, they revealed that PbI_2 heterogeneous cap can also realize $MAPbI_3$ films with large-sized grains [51]. Improved PCE was thus realized because of more efficient transport of charge carriers and decreased non-radiative recombination in corresponding devices. Overall, those works suggest a promising strategy to engineer grain size of metal-halide perovskite films.

In addition to crystallization process control, post-treatment strategies were also developed to engineer grain size of metal-halide perovskite films. For example, obvious grain coarsening via Ostwald ripening in one-step deposited $MAPbI_3$ film can be realized by post-synthesis high-temperature heating treatment assisted with additionally deposited CH_3NH_3I layer [50]. The grain coarsening via Ostwald ripening was revealed to be related to the heating treatment parameters (temperature and time). By optimizing them, the film with average grain size of ~2 μm, much increased crystallinity, and proper stoichiometry can be achieved. Due to those characteristics, defect states along with recombination centers were greatly reduced, and carrier transport and injection properties were much improved. So, efficiency of corresponding planar heterojunction solar cells can be boosted from 14.54 to 16.88%. Then, the same post-treatment recipe was used for thick $MAPbI_3$ films, and a same grain coarsening was observed in them. So post-treatment recipe gives the fact that thickening the absorb layer of cells to realize more sufficient absorption avoids serious aggravation of charge recombination. By further optimizing the thickness of coarsened $MAPbI_3$ films, highly efficient cells

with relatively excellent reproducibility and the optimal efficiency of 19.24% were realized by Yu. et al. [50]. Afterward, a similar MABr treatment converts $MAPbI_3$ thin films to high-quality $MAPbI_{3-x}Br_x$ thin films following an Ostwald ripening process as reported by Zhao et al. [52]. But, they found that similar process is ineffective when replacing MABr with MAI. This phenomenon mainly comes from the fact that low-concentration MAI solution was used and low post-treatment temperature was adopted in their experiments. So, further investigations are needed to clarify those factors. More recently, Jen et al. [53] reported a simple pseudohalide-induced film retreatment technology as passivation for preformed $MAPbI_3$ film. They found that the retreatment process yields a controllable decomposition-to-recrystallization evolution of $MAPbI_3$ film. Corresponding, it remarkably enlarges grain size of the film in all directions, as well as improving crystallinity and hindering trap density.

4.3. Texture engineering of metal-halide perovskite films

As to polycrystalline films, orientation of crystal axis in each grain is another important microstructural feature that dominates their physical properties. Films with aligned crystal axes are so-called textured ones. They possess a single-crystal-like nature along crystal axis, so an enhancement in physical properties is expected for them. In general, ordinarily prepared polycrystalline films are composed of grains with random orientation. Methodology that is explored to develop texture to improve functional properties of polycrystalline films is known as texture engineering. Specifically, one-step deposited metal-halide perovskite films are similarly characterized with randomly oriented grains. Hence, texture engineering is of particular importance to modify their electrical and optical properties, and hence further improve the performance of ultimate cells.

Yan et al. [54] reported that reaction of $HPbI_3$ with low partial pressure MA gas can form a textured $MAPbI_3$ film with high crystallinity. The film exhibits much higher both thermal and moisture stability than the one prepared from MAI + PbI_2. Further investigation revealed that large Pb–N binding energy of ~80.04 kJ mol^{-1} results in a liquefied state after MA adhesion on $MAPbI_3$. And, a highly textured $MAPbI_3$ film is formed when excess MA expeditious are released. Cao et al. [55] found that MACl-containing precursor can yield $MAPbI_3$ film with strong (110) preferred orientation. The $MAPbI_3$ films were used for typical planar solar cells and delivered an impressive average efficiency of 16.63 ± 0.49% and champion efficiency of 17.22%. Yu et al. [56] demonstrated that face-down annealing of one-step deposited precursor films can enable the formation of (110) textured $MAPbI_3$ films consisting of high-crystallinity, well-ordered, micrometer-sized grains that span vertically the entire film thickness, as shown in **Figure 8**. Such microstructural features induced dramatically decreased nonradiative recombination sites as well as greatly improved transport property of charge carries in the films compared with that of the non-textured ones obtained by conventional annealing route. As a consequence, planar heterojunction perovskite solar cells with these textured $MAPbI_3$ films exhibit much improved PCE along with small hysteresis and excellent stability.

4.4. Surface roughness engineering of metal-halide perovskite films

Metal-halide perovskite film was usually sandwiched between electron-transporting layer and hole-transporting layer in perovskite solar cell. And, one of them has to be deposited

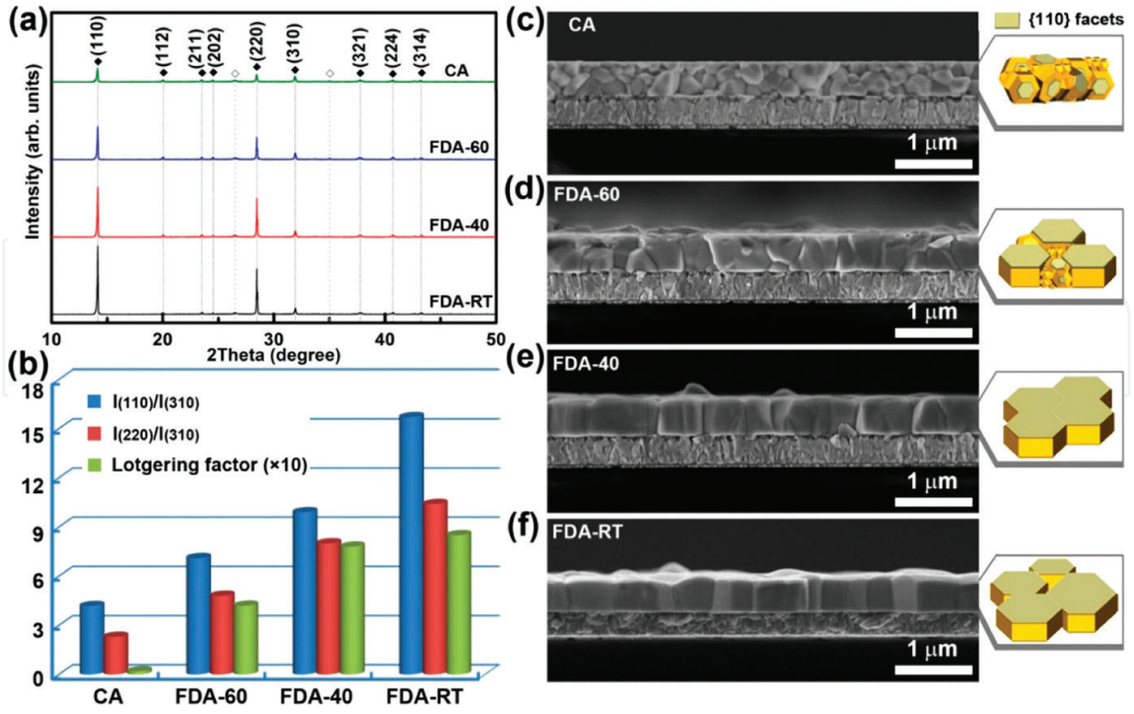

Figure 8. (a) XRD patterns of samples CA, FDA-60, FDA-40, and FDA-RT, respectively. (b) Corresponding histograms of XRD peak intensity ratios of (110) to (310) planes and (220) to (310) planes as well as calculated Lotgering factors. (c–f) cross-sectional SEM images of samples CA, FDA-60, FDA-40, and FDA-RT. Left inset describes the stereoshape model proposed for $MAPbI_3$ grains on TiO_2/FTO substrate. The facets are marked in brown for clarity. The samples with the preheating temperatures of room temperature (RT), 40, and 60°C were labeled as FDA-RT, FDA-40, and FDA-60, respectively. Reproduced with permission from Ref. [56]. Copyright 2017, American Chemical Society.

sequentially on metal-halide perovskite layer. So, surface roughness of metal-halide perovskite film has a significant impact on the cell's interface morphology. A roughened interface that resulted from rough metal-halide perovskite layer would strengthen internal light scattering [57]. And, a large interface area also benefits charge transport [14]. However, high surface roughness of metal-halide perovskite layer will increase short-circuiting possibility of device existing between silver electrode and metal-halide perovskite layer, in the case that electron-transporting layer or hole-transporting layer cannot fully cover the metal-halide perovskite film. In other words, a metal-halide perovskite layer with high roughness requires a thick electron-transporting layer or hole-transporting layer to eliminate short-circuiting. On the contrary, a thin one is preferred to ensure a reasonable FF. So, there is compromise in surface roughness of metal-halide perovskite film as far as cell performance is concerned, and some exploratory works have been undertaken. For example, one the one hand, Meng et al. [58] introduced a hot-pressing method that can transform $MAPbI_3$ film with rough surface to be a smooth one, and pinholes in original film can be cured effectively. This modified $MAPbI_3$ morphology is conductive to improve charge carrier transport and eliminate charge carrier recombination in perovskite solar cells. Moreover, much improved performances with high PCEs of 10.84 and 16.07% are thus realized in hole-transporting-layer-free and spiro-OMeTAD-based cells, respectively. Yu et al. [59] found that spray-assisted process instead of commonly used dipping process in a two-step

spin-coating method can effectively reduce roughness of $MAPbI_3$ films. Experimental results demonstrated that the cells' average V_{oc} can be enhanced from 0.823±0.105 V to 0.940±0.008 V by spray-assisted process. It benefits from low leakage possibility between hole-transport layer and mesoporous TiO_2 layer when a smooth and pinhole-free $MAPbI_3$ has successfully formed. Finally, average PCEs of mesoporous cells could be promoted by 25% approximately. One the other hand, Chen et al. [60] reported a novel $MAPbI_3$ film with a dense under-layer and a porous upper-layer that was formed by using a thin mesoporous TiO_2 seeding layer and a gas-assisted crystallization method. This novel multitiered nanostructure allows for greatly improved light harvesting for wavelengths exceeding 500 nm, as well as a more effective interfacial charge separation for perovskite solar cells. The combination of these factors culminated in average PCEs over 15% and average short-circuit current density exceeded 22 mA cm^{-2}.

5. Conclusions

In summary, metal-halide perovskite films have many excellent optoelectronic properties such as high absorption coefficient, tunable bandgap, long and balanced carrier diffusions, ambipolar transport of charge carriers, tolerance of defects, along with capacity for film deposition via either solution or vacuum-based methods including one-step spin-coating method, sequential deposition method, two-step spin-coating method vacuum coevaporation deposition method, sequential vacuum deposition method, and vapor-assisted solution deposition method. Those desired features make them promising for high-performance and low-cost perovskite solar cells. The microstructural features that mainly refer to surface coverage, grain size, texture, surface roughness, and so on are vital in determining the performance of perovskite solar cells. Specifically, the ones with full surface coverage, large grain size, textured feature, and smooth surface, are highly desirable for efficient devices. Some important progresses in microstructure engineering of metal-halide perovskite films are described in this chapter, which will promote systematically understanding the role of microstructure engineering in the progress of perovskite solar cells.

Acknowledgements

This work was supported primarily by National Natural Science Foundation of China under Grant 61334002 and 61106063, and Class General Financial Grant from the China Postdoctoral Science Foundation (Grant No. 2016M602771).

Conflict of interest

The authors declare no competing financial interest.

Author details

Weidong Zhu*, Jingjing Chang, Chunfu Zhang*, Jincheng Zhang and Yue Hao

*Address all correspondence to: wdzhu@xidian.edu.cn and cfzhang@xidian.edu.cn

Wide Bandgap Semiconductor Technology Disciplines State Key Laboratory, School of Microelectronics, Xidian University, Xi'an, PR China

References

[1] Gao P, Gratzel M, Nazeeruddin MK. Organohalide lead perovskites for photovoltaic applications. Energy & Environmental Science. 2014;**7**(8):2448-2463. DOI: 10.1039/C4EE00942H

[2] Green MA, Ho-Baillie A, Snaith HJ. The emergence of perovskite solar cells. Nature Photonics. 2014;**8**:506-514. DOI: 10.1038/nphoton.2014.134

[3] Correa-Baena JP, Abate A, Saliba M, Tress W, Jesper Jacobsson T, Gratzel M, Hagfeldt A. The rapid evolution of highly efficient perovskite solar cells. Energy & Environmental Science. 2017;**10**(3):710-727. DOI: 10.1039/C6EE03397K

[4] Hörantner MT, Leijtens T, Ziffer ME, Eperon GE, Christoforo MG, McGehee MD, Snaith HJ. The potential of multijunction perovskite solar cells. ACS Energy Letters. 2017;**2**(10):2506-2513. DOI: 10.1021/acsenergylett.7b00647

[5] Yamada Y, Nakamura T, Endo M, Wakamiya A, Kanemitsu Y. Photocarrier recombination dynamics in perovskite $CH_3NH_3PbI_3$ for solar cell applications. Journal of the American Chemical Society. 2014;**136**(33):11610-11613. DOI: 10.1021/ja506624n

[6] Xiao Z, Yuan Y, Wang Q, Shao Y, Bai Y, Deng Y, Dong Q, Hu M, Bi C, Huang J. Thin-film semiconductor perspective of organometal trihalide perovskite materials for high-efficiency solar cells. Materials Science and Engineering Reports. 2016;**101**:1-38. DOI: 10.1016/j.mser.2015.12.002

[7] Park NG. Perovskite solar cells: An emerging photovoltaic technology. Materials Today. 2015;**18**(2):65-72. DOI: 10.1016/j.mattod.2014.07.007

[8] Huang F, Pascoe AR, Wu WQ, Ku Z, Peng Y, Zhong J, Caruso RA, Cheng YB. Effect of the microstructure of the functional layers on the efficiency of perovskite solar cells. Advanced Materials. 2017;**29**(20):1601715. DOI: 10.1002/adma.201601715

[9] Eperon GE, Burlakov VM, Docampo P, Goriely A, Snaith HJ. Morphological control for high performance, solution-processed planar heterojunction perovskite solar cells. Advanced Functional Materials. 2014;**24**(1):151-157. DOI: 10.1002/adfm.201302090

[10] Xiao Z, Dong Q, Bi C, Shao Y, Yuan Y, Huang J. Solvent annealing of perovskite-induced crystal growth for photovoltaic-device efficiency enhancement. Advanced Materials. 2014; **26**(37):6503-6509

[11] Kim HD, Ohkita H, Benten H, Ito S. Photovoltaic performance of perovskite solar cells with different grain sizes. Advanced Materials. 2016;**28**(5):917-922. DOI: 10.1002/adma.201401685

[12] Kim HS, Park NG. Parameters affecting I-V hysteresis of $CH_3NH_3PbI_3$ perovskite solar cells: Effects of perovskite crystal size and mesoporous TiO_2 layer. Journal of Physical Chemistry Letters 2015. 2014;**5**(17):2927-2934. DOI: 10.1021/jz501392m

[13] Bae S, Park JS, Han IK, Shin TJ, Jo WH. $CH_3NH_3PbI_3$ crystal orientation and photovoltaic performance of planar heterojunction perovskite solar cells. Solar Energy Materials & Solar Cells. 2017;**160**:77-84. DOI: 10.1016/j.solmat.2016.10.019

[14] Li G, Ching KL, Ho JYL, Wong M, Kwok HS. Identifying the optimum morphology in high-performance perovskite solar cells. Advanced Energy Materials. 2015;**5**(9):1401775. DOI: 10.1002/aenm.201401775

[15] Fan Z, Sun K, Wang J. Perovskites for photovoltaics: A combined review of organic-inorganic halide perovskites and ferroelectric oxide perovskites. Journal of Materials Chemistry A. 2015;**3**(37):18809-18828. DOI: 10.1039/c5ta04235f

[16] Cui J, Yuan H, Li J, Xu X, Shen Y, Lin H, Wang M. Recent progress in efficient hybrid lead halide perovskite solar cells. Science and Technology of Advanced Materials. 2015;**16**(3):036004. DOI: 10.1088/1468-6996/16/3/036004

[17] Zhang L, Liu X, Li J, McKechnie S. Interactions between molecules and perovskites in halide perovskite solar cells. Solar Energy Materials & Solar Cells. 2018;**175**:1-19. DOI: 10.1016/j.solmat.2017.09.038

[18] Hsiao YC, Wu T, Li M, Liu Q, Qin W, Hu B. Fundamental physics behind high-efficiency organo-metal halide perovskite solar cells. Journal of Materials Chemistry A. 2015;**3**(30):15372-15385. DOI: 10.1039/C5TA01376C

[19] Matthews PD, Lewis DJ, Brie PO. Updating the road map to metal-halide perovskites for photovoltaics. Journal of Materials Chemistry A. 2017;**5**(33):17135-17150. DOI: 10.1039/C7TA04544A

[20] Liyan Y, Alexander TB, David GL, Tao W. Recent progress and challenges of organo-metal halide perovskite solar cells. Reports on Progress in Physics. 2016;**79**(2):026501. DOI: 10.1088/0034-4885/79/2/026501

[21] Miura K, Funakubo H. Electronic structures of tetragonal ABX3: Role of the B-X coulomb repulsions for ferroelectricity and piezoelectricity. In: Barranco AP, editor. Advances in Ferroelectrics. Rijeka: InTech; 2012. pp. 1-24. DOI: 10.5772/52187

[22] Xiao JW, Liu L, Zhang D, De Marco N, Lee JW, Lin O, Chen Q, Yang Y. The emergence of the mixed perovskites and their applications as solar cells. Advanced Energy Materials. 2017;**7**(20):1700491. DOI: 10.1002/aenm.201700491

[23] Stoumpos CC, Kanatzidis MG. The renaissance of halide perovskites and their evolution as emerging semiconductors. Accounts of Chemical Research. 2015;**48**(10):2791-2802. DOI: 10.1021/acs.accounts.5b00229

[24] Stoumpos CC, Malliakas CD, Kanatzidis MG. Semiconducting tin and lead iodide perovskites with organic cations: Phase transitions, high mobilities, and near-infrared photoluminescent properties. Inorganic Chemistry. 2013;**52**(15):9019-9038. DOI: 10.1021/ic401215x

[25] Yin WJ, Yang JH, Kang J, Yan Y, Wei SH. Halide perovskite materials for solar cells: A theoretical review. Journal of Materials Chemistry A. 2015;**3**(17):8926-8942. DOI: 10.1039/C4TA05033A

[26] Koutselas IB, Ducasse L, Papavassiliou GC. Electronic properties of three- and low-dimensional semiconducting materials with Pb halide and Sn halide units. Journal of Physics: Condensed Matter. 1996;**8**(9):1217. DOI: 10.1088/0953-8984/8/9/012

[27] Umebayashi T, Asai K, Kondo T, Nakao A. Electronic structures of lead iodide based low-dimensional crystals. Physical Review B. 2003;**67**(15):155405. DOI: 10.1103/PhysRevB.67.155405

[28] Yin WJ, Shi T, Yan Y. Unique properties of halide perovskites as possible origins of the superior solar cell performance. Advanced Materials. 2014;**26**(27):4653-4658. DOI: 10.1002/adma.201306281

[29] De Wolf S, Holovsky J, Moon SJ, Löper P, Niesen B, Ledinsky M, Haug FJ, Yum JH, Ballif C. Organometallic halide perovskites: Sharp optical absorption edge and its relation to photovoltaic performance. Journal of Physical Chemistry Letters. 2014;**5**(6):1035-1039. DOI: 10.1021/jz500279b

[30] Eperon GE, Stranks SD, Menelaou C, Johnston MB, Herz LM, Snaith HJ. Formamidinium lead trihalide: A broadly tunable perovskite for efficient planar heterojunction solar cells. Energy & Environmental Science. 2014;**7**(3):982-988. DOI: 10.1039/c3ee43822h

[31] McMeekin DP, Sadoughi G, Rehman W, Eperon GE, Saliba M, Hörantner MT, Haghighirad A, Sakai N, Korte L, Rech B, Johnston MB, Herz LM, Snaith HJ. A mixed-cation lead mixed-halide perovskite absorber for tandem solar cells. Science. 2016;**351**(6269):151-155. DOI: 10.1126/science.aad5845

[32] Giorgi G, Fujisawa JI, Segawa H, Yamashita K. Small photocarrier effective masses featuring ambipolar transport in methylammonium lead iodide perovskite: A density functional analysis. Journal of Physical Chemistry Letters. 2013;**4**(24):4213-4216. DOI: 10.1021/jz4023865

[33] Hirasawa M, Ishihara T, Goto T, Uchida K, Miura N. Magnetoabsorption of the lowest exciton in perovskite-type compound (CH_3NH_3)PbI_3. Physica B: Condensed Matter. 1994;**201**:427-430. DOI: 10.1016/0921-4526(94)91130-4

[34] Hu M, Bi C, Yuan Y, Xiao Z, Dong Q, Shao Y, Huang J. Distinct exciton dissociation behavior of organolead trihalide perovskite and excitonic semiconductors studied in the same system. Small. 2015;**11**(18):2164-2169. DOI: 10.1002/smll.201402905

[35] Juarez-Perez EJ, Sanchez RS, Badia L, Garcia-Belmonte G, Kang YS, Mora-Sero I, Bisquert J. Photoinduced giant dielectric constant in lead halide perovskite solar cells. Journal of Physical Chemistry Letters. 2014;**5**(13):2390-2394. DOI: 10.1021/jz5011169

[36] Zheng L, Zhang D, Ma Y, Lu Z, Chen Z, Wang S, Xiao L, Gong Q. Morphology control of the perovskite films for efficient solar cells. Dalton Transactions. 2015;**44**(23):10582-10593. DOI: 10.1039/C4DT03869J

[37] Xiao M, Huang F, Huang W, Dkhissi Y, Zhu Y, Etheridge J, Gray-Weale A, Bach U, Cheng YB, Spiccia L. A fast deposition-crystallization procedure for highly efficient lead

iodide perovskite thin-film solar cells. Angewandte Chemie. 2014;**26**(37):10056-10061. DOI: 10.1002/ange.201405334

[38] Jeon NJ, Noh JH, Kim YC, Yang WS, Ryu S, Seok SI. Solvent engineering for high-performance inorganic–organic hybrid perovskite solar cells. Nature Materials. 2014;**13**:897. DOI: 10.1038/nmat4014

[39] Ahn N, Son DY, Jang IH, Kang SM, Choi M, Park NG. Highly reproducible perovskite solar cells with average efficiency of 18.3% and best efficiency of 19.7% fabricated via Lewis Base adduct of lead(II) iodide. Journal of the American Chemical Society. 2015; **137**(27):8696-8699. DOI: 10.1021/jacs.5b04930

[40] Burschka J, Pellet N, Moon SJ, Humphry-Baker R, Gao P, Nazeeruddin MK, Grätzel M. Sequential deposition as a route to high-performance perovskite-sensitized solar cells. Nature. 2013;**499**:316. DOI: 10.1038/nature12340

[41] Xiao Z, Bi C, Shao Y, Dong Q, Wang Q, Yuan Y, Wang C, Gao Y, Huang J. Efficient, high yield perovskite photovoltaic devices grown by interdiffusion of solution-processed precursor stacking layers. Energy & Environmental Science. 2014;**7**(8):2619-2623. DOI: 10.1039/c4ee01138d

[42] Liu M, Johnston MB, Snaith HJ. Efficient planar heterojunction perovskite solar cells by vapour deposition. Nature. 2013;**501**:395. DOI: 10.1038/nature12509

[43] Chen CW, Kang HW, Hsiao SY, Yang PF, Chiang KM, Lin HW. Efficient and uniform planar-type perovskite solar cells by simple sequential vacuum deposition. Advanced Materials. 2014;**26**(38):6647-6652. DOI: 10.1002/adma.201402461

[44] Chen Q, Zhou H, Hong Z, Luo S, Duan HS, Wang HH, Liu Y, Li G, Yang Y. Planar heterojunction perovskite solar cells via vapor-assisted solution process. Journal of the American Chemical Society. 2014;**136**(2):622-625. DOI: 10.1021/ja411509g

[45] Zhu W, Yu T, Li F, Bao C, Gao H, Yi Y, Yang J, Fu G, Zhou X, Zou Z. A facile, solvent vapor-fumigation-induced, self-repair recrystallization of $CH_3NH_3PbI_3$ films for high-performance perovskite solar cells. Nanoscale. 2015;**7**(12):5427-5434. DOI: 10.1039/c5nr00225g

[46] Zhou Z, Wang Z, Zhou Y, Pang S, Wang D, Xu H, Liu Z, Padture NP, Cui G. Methylamine-gas-induced defect-healing behavior of $CH_3NH_3PbI_3$ thin films for perovskite solar cells. Angewandte Chemie, International Edition. 2015;**54**(33):9705-9709. DOI: 10.1002/anie.201504379

[47] Liu Z, Hu J, Jiao H, Li L, Zheng G, Chen Y, Huang Y, Zhang Q, Shen C, Chen Q, Zhou H. Chemical reduction of intrinsic defects in thicker heterojunction planar perovskite solar cells. Advanced Materials. 2017;**29**(23):1606774. DOI: 10.1002/adma.201606774

[48] Chen H, Ye F, Tang W, He J, Yin M, Wang Y, Xie F, Bi E, Yang X, Grätzel M, Han L. A solvent- and vacuum-free route to large-area perovskite films for efficient solar modules. Nature. 2017;**550**:92. DOI: 10.1038/nature23877

[49] Zhu W, Bao C, Lv B, Li F, Yi Y, Wang Y, Yang J, Wang X, Yu T, Zou Z. Dramatically promoted crystallization control of organolead triiodide perovskite film by a homogeneous

cap for high efficiency planar-heterojunction solar cells. Journal of Materials Chemistry A. 2016;**4**(32):12535-12542. DOI: 10.1039/c6ta04332a

[50] Zhu W, Bao C, Wang Y, Li F, Zhou X, Yang J, Lv B, Wang X, Yu T, Zou Z. Coarsening of one-step deposited organolead triiodide perovskite films via Ostwald ripening for high efficiency planar-heterojunction solar cells. Dalton Transactions. 2016;**45**(18):7856-7865. DOI: 10.1039/C6DT00900J

[51] Wang Y, Li J, Li Q, Zhu W, Yu T, Chen X, Yin L, Zhou Y, Wang X, Zou Z. PbI_2 heterogeneous-cap-induced crystallization for an efficient $CH_3NH_3PbI_3$ layer in perovskite solar cells. Chemical Communications. 2017;**53**(36):5032-5035. DOI: 10.1039/C7CC01573A

[52] Yang M, Zhang T, Schulz P, Li Z, Li G, Kim DH, Guo N, Berry JJ, Zhu K, Zhao Y. Facile fabrication of large-grain $CH_3NH_3PbI_{3-x}Br_x$ films for high-efficiency solar cells via CH_3NH_3Br-selective Ostwald ripening. Nature Communications. 2016;**7**:12305. DOI: 10.1038/ncomms12305

[53] Dong H, Wu Z, Xi J, Xu X, Zuo L, Lei T, Zhao X, Zhang L, Hou X, Jen AKY. Pseudohalide-induced recrystallization engineering for $CH_3NH_3PbI_3$ film and its application in highly efficient inverted planar heterojunction perovskite solar cells. Advanced Functional Materials. DOI: 10.1002/adfm.201704836

[54] Long M, Zhang T, Zhu H, Li G, Wang F, Guo W, Chai Y, Chen W, Li Q, Wong KS, Xu J, Yan K. Textured $CH_3NH_3PbI_3$ thin film with enhanced stability for high performance perovskite solar cells. Nano Energy. 2017;**33**:485-496. DOI: 10.1016/j.nanoen.2017.02.002

[55] Fei C, Guo L, Li B, Zhang R, Fu H, Tian J, Cao G. Controlled growth of textured perovskite films towards high performance solar cells. Nano Energy. 2016;**27**:17-26. DOI: 10.1016/j.nanoen.2016.06.041

[56] Zhu W, Kang L, Yu T, Lv B, Wang Y, Chen X, Wang X, Zhou Y, Zou Z. Facile face-down annealing triggered remarkable texture development in $CH_3NH_3PbI_3$ films for high-performance perovskite solar cells. ACS Applied Materials & Interfaces. 2017;**9**(7):6104-6113. DOI: 10.1021/acsami.6b15563

[57] Zheng L, Ma Y, Chu S, Wang S, Qu B, Xiao L, Chen Z, Gong Q, Wu Z, Hou X. Improved light absorption and charge transport for perovskite solar cells with rough interfaces by sequential deposition. Nanoscale. 2014;**6**(14):8171-8176. DOI: 10.1039/C4NR01141D

[58] Xiao J, Yang Y, Xu X, Shi J, Zhu L, Lv S, Wu H, Luo Y, Li D, Meng Q. Pressure-assisted $CH_3NH_3PbI_3$ morphology reconstruction to improve the high performance of perovskite solar cells. Journal of Materials Chemistry A. 2015;**3**(10):5289-5293. DOI: 10.1039/C4TA06700B

[59] Li F, Bao C, Gao H, Zhu W, Yu T, Yang J, Fu G, Zhou X, Zou Z. A facile spray-assisted fabrication of homogenous flat $CH_3NH_3PbI_3$ films for high performance mesostructure perovskite solar cells. Materials Letters. 2015;**157**:38-41. DOI: 10.1016/j.matlet.2015.05.106

[60] Pascoe AR, Meyer S, Huang W, Li W, Benesperi I, Duffy NW, Spiccia L, Bach U, Cheng YB. Enhancing the optoelectronic performance of perovskite solar cells via a textured $CH_3NH_3PbI_3$ morphology. Advanced Functional Materials. 2016;**26**(8):1278-1285. DOI: 10.1002/adfm.201504190